Transactions of the North American Manufacturing Research Institution of SME Volume 32, 2004

Papers presented at:
NAMRC 32

June 1–4, 2004
The University of North Carolina at Charlotte
Charlotte, North Carolina

Published by the Society of Manufacturing Engineers
in cooperation with the North American Manufacturing Research Institution of SME

One SME Drive, P.O. Box 930, Dearborn, Michigan 48121 USA • www.sme.org

NAMRC 32 organized by The University of North Carolina at Charlotte

A METHOD FOR PREDICTING CHATTER STABILITY FOR SYSTEMS WITH SPEED-DEPENDENT SPINDLE DYNAMICS

Tony L. Schmitz, John C. Ziegert, Charles Stanislaus
Department of Mechanical and Aerospace Engineering
University of Florida
Gainesville, FL

KEYWORDS

Milling, stability, dynamics, rotating

ABSTRACT

Prediction of stable cutting regions is a critical requirement for high-speed milling operations. In practice, these predictions are generally made using measurement of the tool/holder/spindle dynamics obtained from a non-rotating spindle. However, it is known that significant changes in the system dynamics may occur during high-speed rotation. This paper describes an experimental method for the prediction of stable cutting regions which reflects the dynamics of the rotating system.

INTRODUCTION

Research in the area of milling stability has enjoyed a rich history. Early research efforts (Arnold [1946], Tobias [1965], Tobias and Fishwick [1958], Tlusty and Polocek [1963], Koenisberger and Tlusty [1967], and Merrit [1965]) led to mathematical process models and the development of graphical charts, commonly referred to as stability lobe diagrams, that compactly represent stability information as a function of the control parameters, chip width and spindle speed. These studies led to a fundamental understanding of *regeneration of waviness*, or the overcutting of a machined surface by a vibrating cutter, as a primary feedback mechanism for the growth of self-excited vibrations (or chatter) due to the modulation of the instantaneous chip thickness, cutting force variation, and subsequent tool vibration. Many subsequent research efforts have built on this work and the use of stability lobe diagrams, coupled with high-speed/power machining centers and improved cutting tool materials, in production environments has been shown to dramatically increase material removal rates (MRR). For example, high-speed machining has been applied in the aerospace industry, where the dramatic increases in MRR have allowed designers to replace assembly-intensive sheet metal build-ups with monolithic aluminum components resulting in substantial cost savings (Halley *et al.* [1999]).

In general, stability lobe diagrams are developed by selecting the cutting parameters, which include the process-dependent specific cutting energy coefficients, radial immersion, and system dynamics (as reflected at the tool

point), and then carrying out the selected simulation algorithm. In general, the tool point frequency response function (FRF) is measured using impact testing, where an instrumented hammer is used to excite the tool point and the response is measured using an appropriate transducer (often a low-mass accelerometer), while the spindle is stationary, or non-rotating. The underlying assumption here is that the spindle dynamics do not change as the spindle speed is increased. However, any variation in the tool point FRF with changes in spindle speed will directly translate into errors in the stability limit predicted by the selected analysis technique. Potential sources for these variations are described in the following section.

CHANGES IN SYSTEM DYNAMICS WITH SPINDLE SPEED

New spindle designs have significantly contributed to the productivity gains afforded by high-speed milling. These spindles are capable of accommodating tools up to 25 mm in diameter and rotate at speeds of 40000 rpm and higher. Typically, these spindles are directly driven by brushless motors and the spindle shaft is supported by hybrid angular contact bearings with silicon nitride balls. Bearing axial preload is kept essentially constant during thermally-driven changes to the spindle dimensions by spring or hydraulic arrangements. The tool point FRF for these spindles depends on a large number of factors, including tool length (Tlusty *et al.* [1996], Smith *et al.* [1998], Davies *et al.* [1998], Schmitz and Donaldson [2000], Schmitz *et al.* [2001]), holder characteristics (Agapiou *et al.* [1995], Weck and Schubert [1994]), drawbar force (Smith *et al.* [1999]), spindle shaft geometry, and the stiffness and damping provided by the spindle shaft bearings.

While most of these factors are independent of the rotational speed of the spindle, it is known that the radial and axial stiffnesses of angular contact bearings vary with changes in load and speed. This behavior is generally attributed to changes in the contact angles in the inner and outer races due to applied axial and radial loads, and centrifugal and gyroscopic forces on the rotating balls. Any variations in the bearing stiffness with speed will also change the tool point FRF. Therefore, non-rotating measurements of tool point dynamics may not adequately describe the rotating system; furthermore, stability predictions based on these non-rotating measurements may be in error.

Numerous authors have investigated the dynamic behavior of angular contact bearings both analytically and experimentally. Jones [1960] developed a general theoretical model for bearing dynamic loads. Harris [1991] showed that the radial stiffness of angular contact bearings decreases with increasing radial load and speed. Shin [1992] and Chen *et al.* [1994] showed that the dynamic characteristics of the spindle system vary with speed-dependent changes in the bearing stiffness, affecting chatter stability. Chen and Wang [1994] demonstrated the effect of changing end loads on the system dynamics, and describe a method for including the analytically predicted, speed-dependent dynamics in the computation of stability lobes. Jorgenson and Shin [1998] compare analytical predictions of spindle dynamics at speed with experimental measurements.

These authors show that the dynamic response of the tool/holder/spindle/bearing system may not be adequately characterized by non-rotating FRF measurements, and may lead to errors in chatter stability predictions. However, construction of an analytical model of the tool/holder/spindle system dynamics requires detailed knowledge about the geometry and construction of the spindle, which in general is not available to the machine user in a manufacturing environment. Therefore, in this paper we describe a method to develop stability lobe diagrams for the case of speed-dependent spindle dynamics based solely on experimental measurements of the spindle.

SPEED-DEPENDENT STABILITY LOBE DIAGRAMS

In this section we describe the experimental development of stability lobe diagrams that incorporate the dependence of the tool point FRF on spindle speed. We begin with a brief review of the stability analysis technique applied in this research, and then proceed with a description of the method used to construct speed-dependent stability lobe diagrams.

Review of Stability Lobe Diagram Algorithms

Milling stability analyses developed by Tlusty *et al.* (Tlusty *et al.* [1983], Tlusty [1988], Smith and Tlusty [1990], Smith and Tlusty [1991]), Altintas and Budak [1995], and Bayly *et al.* [2001]) are available in the literature. The Tlusty and Altintas and Budak methods analytically transform the time-dependent dynamic milling equations into a time invariant, but radial immersion-dependent system. The Temporal Finite Element Analysis (TFEA) method developed by Bayly *et al.* computes an analytic solution for the cutter displacement when it is not in contact with the workpiece (i.e., under free vibration). When in contact, the time in the cut is broken up into multiple elements and the vector displacement during a single element is approximated as a linear combination of polynomial trial functions. Here, we have used the Altintas and Budak method; however, our analysis technique can generically be applied to each of the three algorithms.

In the Altintas and Budak [1995] approach, the time varying coefficients of the dynamic milling equations, which depend on the angular orientation of the cutter as it rotates through the cut, are expanded into a Fourier series and then truncated to include only the average component. The analytic stability equations provided in this reference have been slightly rearranged here to recast the eigenvalue problem into the form expected by MATLAB™, the computing language used in this study. The *eig.m* MATLAB™ function expects a problem statement in the form det $(A - \lambda I) = 0$, while Altintas and Budak pose the problem as det $(I + \Lambda A) = 0$, where λ and Λ are the system complex eigenvalues for the two formulations, respectively, and A is defined in Eq. 1, where G_x and G_y are the measured x and y-direction tool point FRFs, respectively. The terms α_{xx}, α_{xy}, α_{yx}, and α_{yy} depend on the selected starting and exit angles for the cut and the specific cutting energy coefficient, K_r, which relates the radial cutting force, F_r, to the tangential cutting force, F_t, as shown in Eq. 2. The resulting stability relationships are shown in Eqs. 3-5, where b_{lim} is the limiting chip width or axial depth of cut in peripheral end milling operations, m is the number of cutter teeth, K_t is a second specific cutting energy coefficient that relates F_t to the chip area (i.e., the product of the axial depth of cut, b, and chip thickness, h – see Eq. 2), Ω is the spindle speed in rev/min or rpm, f_c is the chatter frequency (should it occur), and N is an integer that corresponds to the individual lobe numbers (i.e., $N = 0$ is the right-most lobe, $N = 1$ is first lobe to the left, etc.).

$$A = \begin{bmatrix} \alpha_{xx} G_x & \alpha_{xy} G_y \\ \alpha_{xy} G_x & \alpha_{yy} G_y \end{bmatrix} \quad (1)$$

$$F_r = K_r F_t \qquad F_t = K_t b h \quad (2)$$

$$b_{lim} = \frac{2\pi \cdot Re(\lambda)}{m K_t \left(Re(\lambda)^2 + Im(\lambda)^2\right)} \left(1 + \left(\frac{Im(\lambda)}{Re(\lambda)}\right)^2\right) \quad (3)$$

$$\Omega = \frac{2\pi \cdot f_c}{m} \frac{60}{(\gamma + 2\pi \cdot N)} \quad (4)$$

$$\gamma = \pi - 2 \cdot tan^{-1}\left(\frac{Im(\lambda)}{Re(\lambda)}\right) \quad (5)$$

Incorporating FRF Speed Dependence

Using the Altintas and Budak approach, the stability lobe diagram is developed by scanning through the frequency range of interest to determine the complex eigenvalues of the matrix A (Eq. 1) at the selected frequencies. These eigenvalues are then used to determine b_{lim} according to Eq. 3, the phase angle, γ, using Eq. 5, and finally the spindle speed from Eq. 4. Because A is a function of the x and y-direction FRFs, which themselves depend on the selected frequency, the final solution implicitly assumes that G_x and G_y can be used to describe the system behavior over the full range of spindle speeds provided by Eq. 4. For the situation that this is not the case, i.e., the spindle dynamics change with spindle speed, only one point on the computed stability lobe diagram is valid, namely, the spindle speed at which G_x and G_y were measured. In other words, if the non-rotating tool point FRF is used to construct the stability lobe diagram and the system response varies with spindle speed, the only point at which the predicted b_{lim} for that diagram is valid is at zero rpm.

In this situation, it is possible to measure the tool point FRFs in the x and y-directions at a discrete number of spindle speeds, compute the

stability lobe diagram at each spindle speed using the corresponding FRFs, select the predicted b_{lim} at the appropriate spindle speed for each case, and use these points to construct a new diagram that now incorporates the FRF speed dependence. One caveat to these measurements is that testing must be carried out with adequate spindle speed resolution to capture the complicated stability behavior. A graphical description of these steps is provided in Fig. 1.

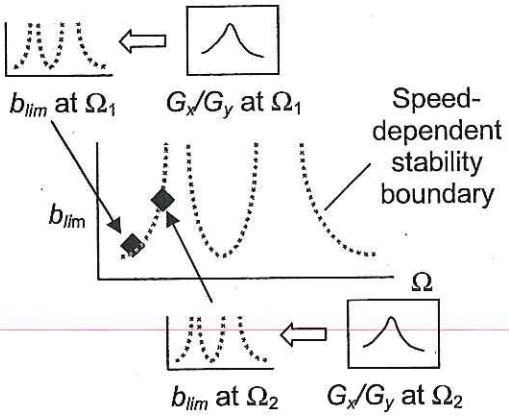

FIGURE 1. DEVELOPMENT OF SPEED-DEPENDENT STABILITY LOBE DIAGRAMS.

MEASUREMENT OF SYSTEM DYNAMICS DURING SPINDLE ROTATION

The rotating tool FRF measurement setup is shown in Fig. 2. The 19.05 mm diameter, 102 mm overhang, three flute, high-speed steel cutting tool was clamped in a CAT-40 tool holder and mounted in a 36000 rpm/36 kW direct drive, rolling element bearing spindle. The spindle shaft was supported by two pairs of hybrid angular contact bearing (silicon nitride balls with steel races); a floating mount carried the rear bearings, with the axial preload provided by a stack of Bellville washers. An instrumented hammer was used to excite the tool at a location below the flute length (approximately 28 mm from the tool free end) and the response was recorded using a capacitance probe (25 μm/V sensitivity). The force and vibration signals were amplified and then recorded using a dynamic signal analyzer. The excitation bandwidth for all cases was approximately 3 kHz. Measurements were performed at 1000 rpm increments from 10000 rpm to 28000 rpm. To minimize potential variations in assembly dynamics, the tool and holder were not removed from the spindle during testing.

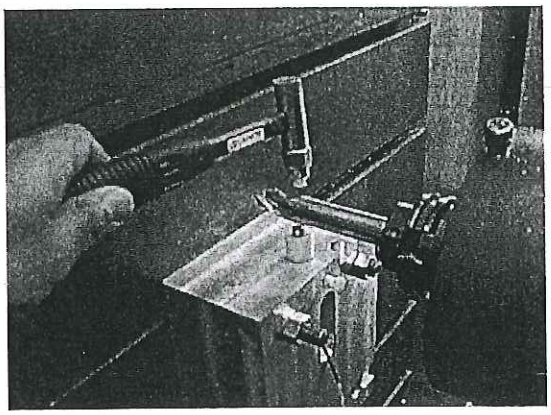

FIGURE 2. ROTATING TOOL FRF MEASUREMENT SETUP.

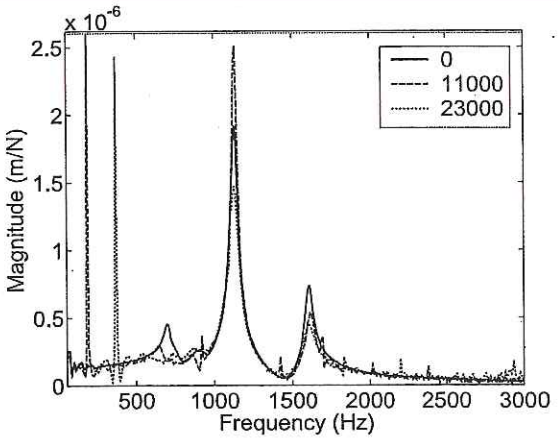

FIGURE 3. FRF COMPARISON FOR 0 RPM, 11000, RPM, AND 23000 RPM CASES.

Example FRF measurements for the x-direction (feed direction for the cutting tests) recorded at 0 rpm, 11000 rpm, and 23000 rpm are shown in Fig. 3, where each measurement is composed of 15 averages and the response magnitude, $\left|\frac{X}{F}\right|$, is plotted. A comparison of the dynamic stiffness for the dominant tool mode at 1128 Hz reveals the following: 1) when comparing the 0 rpm and 11000 rpm tests, the peak-to-peak amplitude increases from 1.9×10^{-6} m/N to 2.5×10^{-6} m/N (reduced dynamic

stiffness); and 2) between the 11000 rpm and 23000 rpm tests, the amplitude decreases from $2.5x10^{-6}$ m/N to $1.4x10^{-6}$ m/N (increased dynamic stiffness). No corresponding shift in the natural frequency is observed. For the spindle mode at 1608 Hz, the amplitude decreases from $7.4x10^{-7}$ m/N to $5.4x10^{-7}$ m/N and $4.5x10^{-7}$ m/N as the spindle speed is increased from 0 rpm to 11000 rpm and, finally, 23000 rpm. The corresponding natural frequencies are 1608 Hz, 1616 Hz, and 1600 Hz, respectively.

Measurement Issues

There were several considerations that had to be addressed during the rotating tool FRF measurements. First, the measurement setup described in the previous paragraph does not provide the tool point FRF required for stability analysis. To obtain this data, it was assumed that, although the amplitude of vibration may vary, the mode shapes do not change appreciably with spindle speed. Therefore, non-rotating FRFs were measured at both the tool point and the rotating FRF measurement location. For each mode within the measurement bandwidth, the amplitude ratio between the two locations was determined. These ratios were then used to project the rotating FRFs to the tool point for the stability lobe development. The agreement between predicted stability lobes and cutting tests (see Experimental Verification section) suggests that this approximation is reasonable, if not entirely accurate.

A second critical measurement issue was tool runout. First, if the amplitude was too high, the full dynamic range of the capacitance probe was expended on runout alone. It was found that mounting the ground tool in the thermal shrink-fit holder provided acceptable shank runout levels in this case. Second, the fundamental runout frequency and its harmonics appeared in the measured FRFs and would artificially affect the computed stability lobes if not treated. For example, the fundamental runout frequencies for the 11000 rpm and 23000 rpm tests, 183 Hz and 283 Hz, respectively, are seen in Fig. 3. Therefore, modal fits were performed to capture the dynamic behavior and remove the runout effects. The modal fits also served to reduce the overall measurement noise generated by the spindle, lubrication system, and machine.

Stability Lobe Diagram Comparison

Stability lobe diagrams were constructed using both the non-rotating FRF and the method described previously that incorporates the FRF speed dependence shown in Fig. 3. These results are presented in Fig. 4 for a slotting cut in the x-direction (specific cutting energy coefficients were K_t = 670 N/mm^2 and K_r = 0.26 for the 6061-T6 aluminum used in this study). In Fig. 4, the stability limits are shown as discrete values at the rotating FRF spindle speeds; for comparison purposes, the limiting axial depths were also calculated at the same spindle speeds for the non-rotating FRF stability lobes, although the full stability boundary was available analytically. In both cases, line segments connect the individual points as a guide to the eye. It is seen that for the 18000 rpm to 28000 rpm spindle speed range, the stability limits predicted from the rotating FRFs are significantly higher due to the increased dynamic stiffness for this range shown in Fig. 3.

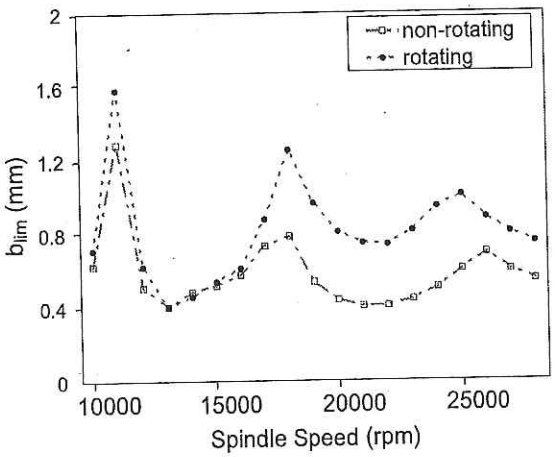

FIGURE 4. COMPARISON OF NON-ROTATING AND ROTATING FRF STABILITY LOBE DIAGRAMS.

EXPERIMENTAL VERIFICATION

The machining setup is shown in Fig. 5. Slots were milled at varying axial depths and spindle speeds in the x-direction using a constant chip load of 0.1 mm/tooth. During the cuts, the sound signal was recorded using a unidirectional microphone (22 kHz sampling frequency).

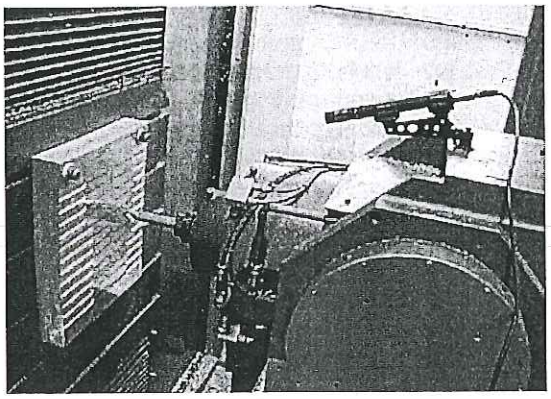

FIGURE 5. MACHINING TEST SETUP, INCLUDING UNIDIRECTIONAL MICROPHONE.

Chatter Determination

In order to compare cutting test results to the predicted stability lobes, it was necessary to experimentally identify stable and unstable cuts. As outlined by Delio *et al.* [1992] and Winfough and Smith [1995], by observing the spectrum of the sound recorded during the cut (i.e., the content of the signal Fourier transform) it is possible to identify unstable cutting conditions. In this method, the runout frequency, f_{ro}, and its harmonics, as well as the tooth passing frequency, f_t, and its harmonics are identified and comb-filtered. Any remaining peak, in the absence of external noise sources, is then identified as a chatter frequency. Because this method requires that a noise threshold be identified (above which chatter is recognized), it was combined with subjective impressions during the cut and visual interpretation of the machined surface quality to identify the boundary between stable and unstable cuts. Example frequency content and photographs of the machined surfaces for stable and unstable cuts at 21000 rpm are shown in Fig. 6. The runout and tooth passing frequencies, as well as their harmonics, are identified. For the unstable cut, the chatter frequency at 1585 Hz is also specified.

Cutting Test Results

Figure 7 shows the non-rotating and rotating stability boundaries from Fig. 4 (only the line segments between points are shown) with the test results superimposed. In this figure stable cuts are identified by solid circles, unstable cuts by crosses (x), and marginally stable cuts by open squares. Improved stability is seen at speeds of 16000 rpm and higher; this agrees with the increased dynamic stiffness recorded between 11000 rpm and 23000 rpm in Fig. 3. The agreement between the cutting tests and predicting rotating FRF stability lobes is reasonable, but the actual stability limit is under-predicted in the region between 16000 rpm and 18000 rpm. Because the lobe peaks are actually the intersection of vectors from successive *N*-number lobes, this region is sensitive to variations in damping. Therefore, slight errors in the modal fits applied to the measured rotating FRFs could account for the disagreement seen here. Additionally, decreasing the spindle speed increment between FRF measurements may lead to a more accurate representation of the overall stability behavior.

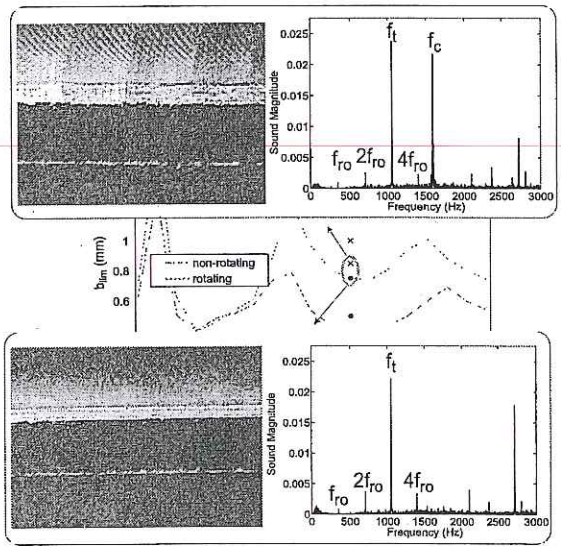

FIGURE 6. STABILITY DETERMINATION BY SPECTRUM EVALUATION AND SURFACE QUALITY.

CONCLUSIONS

In this paper we presented non-rotating and rotating tool FRF measurements that demonstrate a dependence of dynamic stiffness on spindle speed. These FRFs were then used to construct the speed-dependent stability boundaries by analytically computing the stability limit obtained from stability lobe diagrams separately generated for each FRF result, and then organizing these individual points into a single new stability lobe diagram.

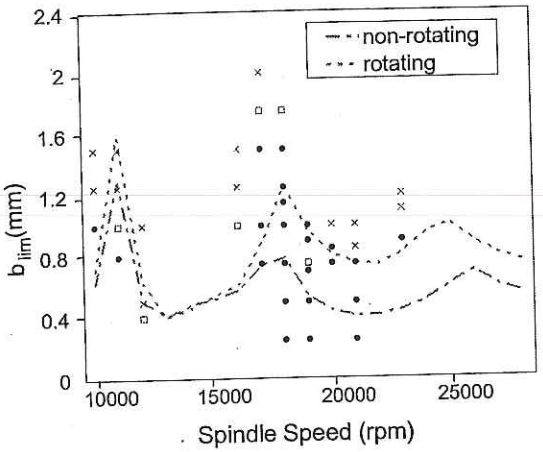

FIGURE 7. MACHINING TEST RESULTS.

It was shown that for the direct drive, rolling element bearing spindle studied here, the dynamic stiffness increased at higher spindle speeds. Therefore, the stability lobe diagram generated from the non-rotating FRF measurement under-predicted the allowable depth of cut. A comparison between the non-rotating and speed-dependent stability lobe diagrams and test cuts demonstrated the expected increased stable cutting depths at higher speeds and validated the approach outlined in this paper.

ACKNOWLEDGEMENTS

This material is partially supported by the National Science Foundation under Grants No. DMI-0000009 and DMI-0238019. Any opinions, findings, and conclusions or recommendations expressed in this material are those of the authors and do not necessarily reflect the views of the National Science Foundation.

The authors also acknowledge helpful discussions with Mr. J. Halley, Tech Manufacturing, Wright City, MO, and Dr. S. Smith, University of North Carolina-Charlotte, Charlotte, NC, regarding variations in spindle dynamics with changes in spindle speed.

REFERENCES

Agapiou, J., E. Rivin, and C. Xie, (1995), "Toolholder/Spindle Interfaces for CNC Machine Tools", *Annals of the CIRP*, Vol. 44/1, pp. 383-387.

Altintas, Y., and E. Budak, (1995), "Analytical Prediction of Stability Lobes in Milling", *Annals of the CIRP*, Vol. 44-1, pp. 357-362.

Arnold, R. N., (1946), "The Mechanism of Tool Vibration in the Cutting of Steel", *Proceedings of the Institution of Mechanical Engineers*, Vol. 154- 4, pp. 261-284.

Bayly, P., J. Halley, B. Mann, and M. Davies, (2001), "Stability of Interrupted Cutting by Temporal Finite Element Analysis", *Proceedings of the 18th Biennial Conference on Mechanical Vibration and Noise*, DETC2001/VIB-21581, ASME Design Engineering Technical Conferences, September 9-13, Pittsburgh, PA.

Chen, C., K. Wang, and Y. Shin, (1994), "An Integrated Approach Toward the Dynamic Analysis of High-Speed Spindles, Part 1: System Model", *ASME J. of Vibrations and Acoustics*, Vol. 116, pp. 506-513.

Chen, C.H., and K. Wang, (1994), "An Integrated Approach Toward the Dynamic Analysis of High-Speed Spindles, Part 2: Dynamics Under Moving End Load", *ASME J. of Vibrations and Acoustics*, Vol. 116, pp. 514-522.

Davies, M., B. Dutterer, J. Pratt, and A. Schaut, (1998), "On the Dynamics of High-Speed Milling with Long, Slender Endmills", *Annals of the CIRP*, Vol. 47/1, pp. 55-60.

Delio, T., J. Tlusty, and S. Smith, (1992), "Use of Audio Signals for Chatter Detection and Control", *Journal of Engineering for Industry*, Vol. 114, pp. 146-157.

Halley, J., A. Helvey, S. Smith, and W. Winfough, (1999), "The Impact of High-Speed Machining on the Design and Fabrication of Aircraft Components", *Proceedings of the 17th Biennial Conference on Mechanical Vibration and Noise*, 1999 ASME Design and Technical Conferences, Las Vegas, Nevada, September 12-16.

Harris, T., (1991), *Rolling Bearing Analysis, 3rd Ed.*, Wiley Interscience.

Jones, A., (1960) "A General Theory for Elastically Constrained Ball and Radial Roller

Bearings under Arbitrary Load and Speed Conditions", *ASME J. of Basic Engineering,* Vol. 82, pp. 309-320.

Jorgenson, B., and Y. Shin, (1998), "Dynamics of Spindle-Bearing Systems at High Speeds Including Cutting Load Effects", *ASME J. of Manufacturing Sciences and Engineering,* Vol. 120, pp. 387-394.

Koenisberger, F., and J. Tlusty, (1967), *Machine Tool Structures-Vol. I: Stability Against Chatter*, Pergamon Press.

Merrit, H., (1965), "Theory of Self-Excited Machine Tool Chatter", *Journal of Engineering for Industry*, Vol. 87-4, pp. 447-454.

Schmitz, T., M. Davies, and M. Kennedy, (2001), "Tool Point Frequency Response Prediction for High-Speed Machining by RCSA", *Journal of Manufacturing Science and Engineering*, Vol. 123, pp. 700-707.

Schmitz, T., and R. Donaldson, (2000), "Predicting High-Speed Machining Dynamics by Substructure Analysis", *Annals of the CIRP*, Vol. 49/1, pp. 303-308.

Shin, Y., (1992), "Bearing Nonlinearity and Stability Analysis in High-Speed Machining", *ASME J. of Engineering for Industry*, Vol. 114, pp. 23-30.

Smith, S., P. Jacobs, and J. Halley, (1999), "The Effect of Drawbar Force on Metal Removal Rate in Milling", *Annals of the CIRP*, Vol 48/1, pp. 293-296.

Smith, S., and J. Tlusty, (1990), "Update on High-Speed Milling Dynamics", *Journal of Engineering for Industry*, Vol. 112, pp. 142-149.

Smith, S., and J. Tlusty, (1991), "An Overview of Modeling and Simulation of the Milling Process", *Journal of Engineering for Industry*, Vol. 113, pp. 169-175.

Smith, S., W. Winfough, and J. Halley, (1998), "The Effect of Tool Length on Stable Metal Removal Rate in High-Speed Milling", *Annals of the CIRP*, Vol. 47/1, pp. 307-310.

Tlusty, J., (1985), "Dynamics of High-Speed Milling", *Handbook of High-Speed Machining Technology*, R. I. King, ed., Chapman and Hall, New York, pp. 48-153.

Tlusty, J., and M. Polocek, (1963), "The Stability of the Machine-Tool against Self-Excited Vibration in Machining", *Proceedings of the International Research in Production Engineering Conference*, Pittsburgh, PA, pp. 465.

Tlusty, J., S. Smith, and W. Winfough, (1996), "Techniques for the Use of Long Slender End Mills in High-Speed Machining", *Annals of the CIRP*, Vol. 45/1, pp. 393-396.

Tlusty, J., W. Zaton, and F. Ismail, (1983), "Stability Lobes in Milling", *Annals of the CIRP*, Vo. 32-1, pp. 309-313.

Tobias, S. A., (1965), *Machine-Tool Vibration*, Blackie and Sons Ltd., Glasgow, Scotland.

Tobias, S. A., and W. Fishwick, (1958), "Theory of Regenerative Machine Tool Chatter", *The Engineer*, Vol. 205.

Weck, M., and I. Schubert, (1994), "New Interface Machine/Tool: Hollow Shank", *Annals of the CIRP*, Vol. 43/1, pp. 345-348.

Winfough, W., and S. Smith, (1995), "Automatic Selection of the Optimum Metal Removal Conditions for High-Speed Milling", *Transactions of the NAMRI/SME*, Vol. 23, pp. 163-168.